Journal of Engineering and Applied Sciences 12 (Special Issue 6): 7912-7918, 2017
ISSN: 1816-949X

Structural and Surface Roughness Effects on Sensing Properties of ZnO Doping with Al Thin Films Deposited by Spray Pyrolysis Technique

[1]Mohammed Ahmed Mohammed and [2]Saba Razaq Salman
[1]University of Al-Qadisiyah, College of Agriculture, Al Diwaniyah, Iraq
[2]University of Babylon, College of Education for Pure Sciences, Hillah, Iraq

Abstract: In this study, the gas sensor properties of ZnO doping with (2 and 4 wt%). Al thin films have been accounted for where the nanocrystalline ZnO based thin films were all around kept by a straight forward and Chemical Spray Pyrolysis (CSP) system. Films have been observed to be uniform, pinhole free and well disciple to the substrate. The morphology, structures and surface harshness of the stored Al doped ZnO thin films were contemplated by different sorts of portrayal strategies. The creators have watched that the sensor reaction and selectivity towards CO gas is enhanced by the Al doping at a low temperature. XRD showed that the acquired films are nanocrystalline in nature with hexagonal wurtzite phase. The films were utilized for identification of CO noticeable all around and most extreme reaction was seen at 175°C. The change in sensor response of ZnO:Al thin films to CO gas credited to the imperfection chemistry, crystallite size and surface" roughness.

Key words: ZnO:Al , gas sensor, thin films, chemical spray pyrolysis, hexagonal, roughness

INTRODUCTION

Metal Oxides (MOs) have picked up an impressive research enthusiasm because of its minimal effort and straightforward handling steps and high potential for the electronic and optoelectronic applications (Huang *et al*., 2012; Vasilopoulou *et al*., 2011; Hasan and Mohammed 2015; Fan *et al*., 2013). The advance in the field of using MOs for gas detecting application was highlighted by the high detecting capacities of MOs and their physical properties, for example, electrical transport, attractive, optical reaction, warm conductivity and superconductivity (Masuda *et al*., 2015; Gaspera *et al*., 2012; Diyatmika *et al*., 2015; Cao and Wu, 2011; He and Wang, 2015). The MOs semiconductor materials have been broadly examined in gas detecting applications because of their simplicity of recognition both oxidizing and decreasing gasses. Among different MOs semiconductors, ZnO is an immediate, wide band crevice (Eg = 3.37 eV at room temperature) and most encouraging multifunctional material in view of its plenitude in nature, more affordable and has high exciton restricting vitality of 60 me V which makes the exciton state stable, even at room temperature (Willander *et al*., 2012; Benharrats *et al*., 2010). Moreover, its biodegradable and biocompatible properties likewise make it a reasonable contender for different applications (Huang *et al*., 2011; Djurisic *et al*., 2012; Li *et al*., 2008, 2015; Hameed *et al*., 2016; Tang *et al*., 2010; Lin *et al*., 2013; Wang *et al*., 2014; Chen *et al*., 2015).

ZnO based electronic gadgets, for example, gas sensors are anticipated to be a superior worker and empower the new capacities (Zhang *et al*., 2016). Besides, the streamlined doped ZnO thin film has a tremendous potential for understanding the detecting properties and their working component. Be that as it may, the negative and less uncovered surface territory of ZnO nanostructure ought to be controlled amid the amalgamation procedure to improve the detecting capacity. In this way, to blend and investigate the detecting conduct of the doped ZnO nanostructure and to additionally comprehend the bits of knowledge of detecting component is one of the points of the present reviews.

The doped and un-doped nanostructures of the ZnO thin films have been orchestrated with using a few techniques, for example, sputtering (Yang *et al*., 2008), sol gel (Tsay and Hsu, 2013) and spin coating (Poongodi *et al*., 2015), etc. The basic element between the said procedures is the necessity of complex and controlled condition that prompts an expansion in cost and intricacies all the while. Be that as it may, a non-vacuum based (CSP) prepare, a non-vacuum process is more helpful, alongside minimum costly and reasonable for substantial territory of affidavit (Kumar *et al*., 2014). One of the upsides of this procedure in regards to doping of tests is that it is anything but difficult to dope the specimens of any component whose salt can be disintegrated in the shower arrangement. The developing worldwide worry for ecological security, contamination and its impacts have invigorated the consideration of the exploration group in the creating field of gas sensor. CO is generally created in transportations and mechanical apparatuses and it is perilous in nature

Corresponding Author: Mohammed Ahmed Mohammed, University of Al-Qadisiyah, College of Agriculture, Al Diwaniyah, Iraq

and its spillage recognition is likewise a critical issue. The ues of the MOs for gas detecting has been generally considered. In any case, the testimony of nanocrystalline thin films of Al-doped ZnO and their morphological and basic impact on gas detecting properties are once in a while found in the writing.

In the present review, we report the amalgamation of ZnO and Al-doped ZnO based thin films by a basic and cheap strategy, i.e., CSP and it is described to assess its gas detecting properties. Structure and surface morphology of the films were researched by (XRD), (AFM) and Scanning Electron Microscopy (SEM). The sensor reactions of unadulterated and Al-doped ZnO movies were contemplated for CO gas. The impact of working temperature on sensor response of kept films towards CO introduction is discussed.

MATERIALS AND METHODS

Pure and doped ZnO:Al films on a glass substrate were deposited by CSP technique. Zn $(CH_3COO)_2$. $2H_2O$ and $AlCl_3 \cdot 6H_2O$ was utilized as source materials for the testimony of thin films. Glass substrates were cleaned with water, then washed with ethanol, then using ultrasonic cleaner. About 0.1 M forerunners were dissolved in ethanol. Al doping concentration changed from 2-4 wt%. The mixing was utilizing using an ultra-sonication for 20 min. The resulting solution was sprayed onto the glass substrate by atomizer. The deposition temperature was maintained at 400°C. The distance between the substrate and atomizer was 30 cm.

Characterization: X-ray diffraction investigation was utilized to perceive the precious stone structure of ZnO pure and doped films using X-ray diffraction instrument type (Shimadzu 6000) with wavelength of 1.5045 Å and the scanning range 20-80°. Surface topography of these films was studied by Atomic Force Microscopy (AFM) using a Digital Instruments, Inc. BY3000. The morphology of thin films was examine by Scanning Electron Microscopy (SEM) type inspect 550. Gas sensing experiments were performed with were measured by using homemade equipment at an operating temperature 100-300°C.

RESULTS AND DISCUSSION

Figure 1 portrays the XRD of ZnO pure and doped thin films . The got diffraction of tests films are hexagonal crystal structure of ZnO (JCPDS card document 36-1451). From the indicated XRD design in Fig. 1, it is watched that intensity of the peak decreases with Al fuse in ZnO lattice and width has turned out to be more extensive approving little grain formation. Closely, this behavior has been earlier reported by Kim *et al.* (2000).

The crystallite sizes (D) of the ZnO:Al thin films was employed by using Scherer's formula and is given by:

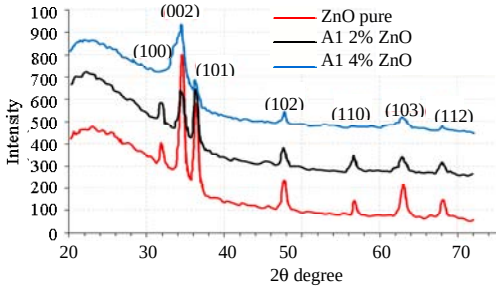

Fig. 1: XRD pattern of ZnO:Al thin films

$$D = \frac{k\lambda}{\beta\cos\theta} \quad (1)$$

Where:

k = 0.94 (constant)

λ = Wavelength of the X-ray equal 1.54 Å

β = The Full Width at Half Maxima (FWHM) (in radians) of the diffraction peak

The average crystallite size of films was found in Table 1. Note that the average of grain size decrease with increasing Al wt.%, this shows a development in the structural properties of the films.

Additionally, for more information on the amount of defects in the thin films, the number of layerss (Nl), micro strainss (ε), dislocation densitys (δ), Specific Surface Area (SSA) (Mandal *et al*., 2006) and Texture coefficient $T_{c(hkl)}$ (Nasser *et al*., 1998) were evaluated as shown in Table 2 from Eq. 2-6, respectively:

$$N_l = \frac{t}{D^3} \quad (2)$$

$$\varepsilon = \frac{\beta\cos\theta}{4} \quad (3)$$

$$\delta = \frac{1}{D^2} \quad (4)$$

$$SSA = \frac{6000}{D\times\rho} \quad (5)$$

Where ρ is bulk density for ZnO equal 0.88 g/cm^3:

$$T_{c(hkl)} = \frac{I_{(hkl)}/I_{o(hkl)}}{(1/N)\left[\sum_N I_{(hkl)}/I_{o(hkl)}\right]} \quad (6)$$

Where:

$T_{c(hkl)}$ = The texture coefficient of the hkl plane

$I_{(hkl)}$ = The measured intensity

$I_{o(hkl)}$ = The relative intensity of the corresponding plane given in PDF-2 data and N is the number of reflections

Table 1: XRD parameters for ZnO:Al thin films

Samples/(hkl)	2θ (deg)	θ (deg)	d (nm)	FWHM (rad)	GS (nm)	Average GS (nm)
ZnO pure						
100	31.8	15.90	0.28106373	0.01517566	9.91842620	9.42144485
002	34.0	17.00	0.26336338	0.01593444	9.49982100	
101	36.0	18.00	0.24917723	0.01669322	9.11805119	
102	47.8	23.90	0.19005701	0.01896957	8.34688012	
110	57.0	28.50	0.16137187	0.01972836	8.34947521	
103	63.0	31.50	0.14736883	0.01972836	8.60581286	
112	68.0	34.00	0.13769846	0.01441688	12.11164740	
ZnO:2% Al						
100	32.0	16.00	0.27935256	0.01669322	9.02124992	8.60410675
002	35.0	17.50	0.25606423	0.01896957	8.00150207	
101	36.5	18.25	0.24587771	0.01669322	9.13108348	
102	47.5	23.75	0.19118717	0.01745201	9.06221345	
110	57.0	28.50	0.16137187	0.01972836	8.34947521	
103	63.0	31.50	0.14736883	0.02276349	7.45837115	
112	68.0	34.00	0.13769846	0.01896957	9.20485200	
ZnO:4% Al						
002	35.0	17.50	0.25606423	0.01896957	8.00150207	8.57160443
101	36.5	18.25	0.24587771	0.01669322	9.13108348	
102	47.5	23.75	0.19118717	0.01745201	9.06221345	
103	63.0	31.50	0.14736883	0.02276349	7.45837115	
112	68.0	34.00	0.13769846	0.01896957	9.20485200	

Table 2: Numbers of Layers (Nl)s, micro strain (ε), dislocationsdensity (δ), Specific Surface Areas (SSA) and Texture coefficient Tc (hkl) for ZnO:Al thin films

Samples	Average$N_l \times 10^{17}$ (m^{-2})	Average ε (%)	Average $\delta \times 10^{16}$ (m^{-2})	SSA (m^2/g)	I	I_o	avg. $T_{c(hkl)}$
ZnO pure	1.23227	0.00389	1.17559	723.687	400	410	0.123227
					800	810	
					650	610	
					290	300	
					150	160	
					210	200	
					160	165	
ZnO:2% Al	1.54467	0.00423	1.3743	792.433	590	580	0.154467
					650	650	
					660	670	
					390	400	
					360	340	
					360	370	
					320	310	
ZnO:4% Al	1.4943	0.00425	1.39137	795.438	950	930	0.1564
					700	710	
					580	560	
					510	520	
					160	165	

From Table 2, the variation of layer number varies with pure and doped thin films in a random way. It is thought that the quantity of drop plays a greats role in this random change. The micro strain depends directly on the lattice constant (c) and its value related to the shift from the JCPDS file No. 36-1451 value. The values of micro strain increase with increasing Al wt% in the films. The dislocation density is the measure of amount of defects in a crystal. Note the value of average dislocation density obtained in the present research decreases with increase of Al wt%. This confirmed good crystallinity of prepared thin films.

Also, from Table 2 shows increase specific surface area and texture coefficient with increase of Al wt%. The surface of the synthesized materials is found to be very large and hence, the heterogeneous catalytic property of the material were tested and found positive response.Encourage, the defect chemistry of these films was calculated from the XRD. Varieties of Δd/d with

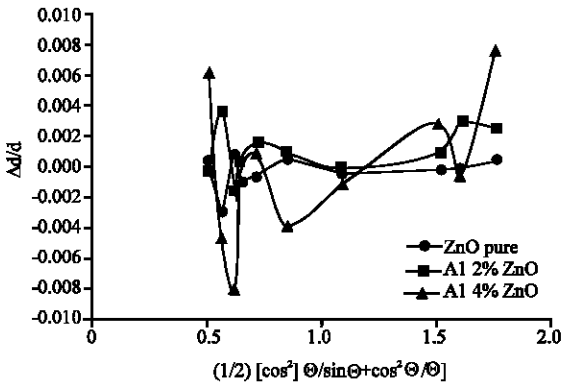

Fig. 2: Δd/d vs. Nelson-Riley Factor (NRF) for ZnO:Al thin films

Nelson-Riley Factor (NRF) (Kaur *et al*., 2007) for ZnO:Al (2 and 4 wt%) films is appeared in the Fig. 2. The standard

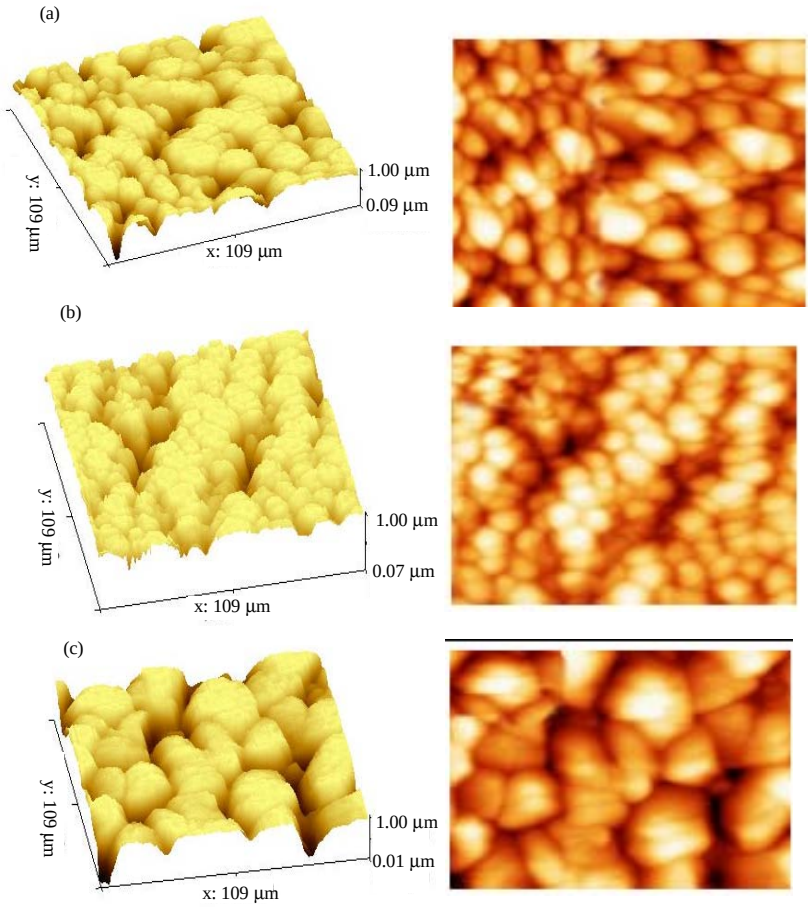

Fig. 3: AFM images of; a) ZnO Pure; b) ZnO:2% Al and c) ZnO:4% Al thin films

information for d-separating estimations of ZnO were taken from JCPDS record No. 36-1451. It is watched that with an expansion in aluminum convergence of the films, scattered-ness of Δd/d values increase. It derives the presentation of stacking shortcomings with the joining of various grouping of aluminum in ZnO films. Subjectively, the scattered-ness of Δd/d values show the thickness of stacking issues exhibit in the films (Kaur *et al*., 2007). It can in this way, be construed that aluminum joining prompts an expansion in the stacking issue thickness of the ZnO thin films with an increase in the lattice parameter.

The morphology and microstructure of the surface of the ZnO:Al thin films were examined by the AFM. The ZnO:Al films are appeared in Fig. 3. The surface morphologies for various doping centralizations of the films appear to be dense, the topography pictures nearly don't show any changes and make known good quality films. The smooth surface was plainly observed for ZnO pure an increasing in Al add up to ZnO lattice appeared with a high surface roughness. The 4 wt% Al doped ZnO thin films, showed that the littler particles agglomerated and made bigger globules particles as as compares to another. Subsequently, these results favor the shape distortion of crystallites in Al dopeds ZnO thin filmssascribed to all the more stacking defects display in the films. The Root Mean Squares (RMS) roughness of thin films with 0. 2 and 4% Al are 14, 17 and 20 nm. These results are like different reports (Kaur *et al*., 2007; Schmidt-Mende and MacManus-Driscoll, 2007).

Figure 4 appear the SEM image of the ZnO:Al thin. The micrograph obviously modulation in the average grain size with an increase in Al wt%. Figure 4 demonstrates that the thin films are uniform and grains are around circular in nature. Both the XRD image and the SEM micrographs infer that the expansion of Al in ZnO grid confines the development of grains. The normal grain measure seen if there should be an occurrence of the immaculate ZnO film was around 95 nm and found to diminish ~40 and ~23 nm for 2 and 4 wt% Al.

The evaluated crystallite sizes utilizing Scherer's equation and from SEM micrographs for ZnO:Al films are not comparable with each other, it might be expected to the presence of indistinct stage around the grains.

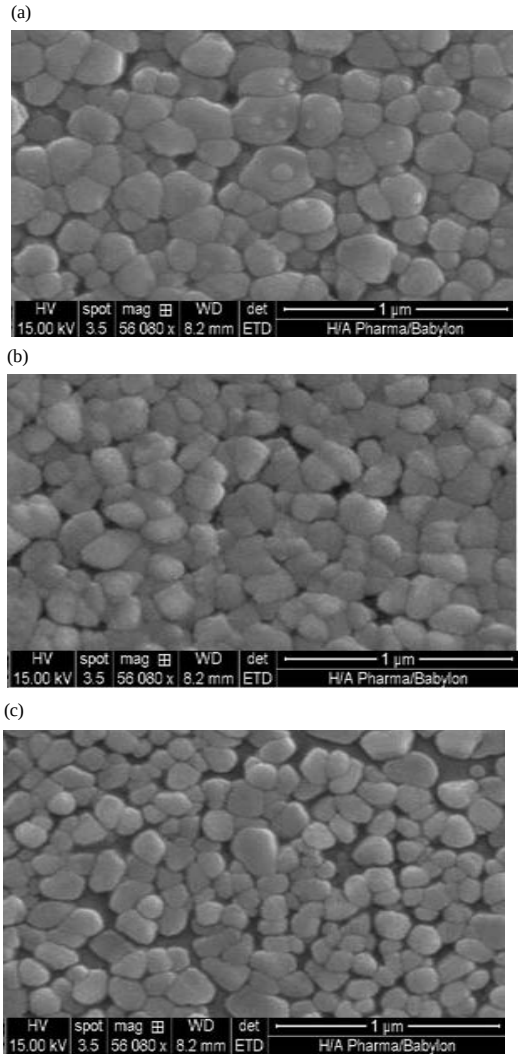

Fig. 4: SEM images of; a) ZnO Pure; b) ZnO:2% Al and c) ZnO:4% Al thin films

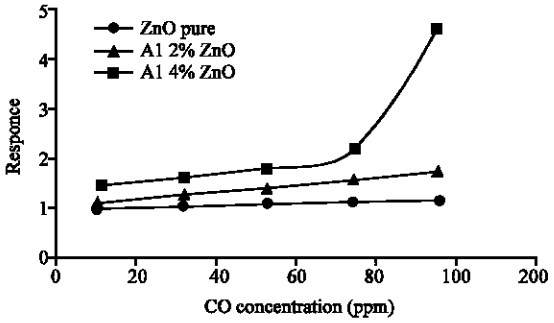

Fig. 5: Sensor response vs. CO concentration for ZnO:Al thin films

Figure 5 shows sensor response with CO concentration, it has been watched that the 4 wt% ZnO:Al sensor showed the most extreme affectability to CO when contrasted with another. The sensor reaction increments with CO concentration up to 100 ppm and sensor reaction immersed past 100 ppm of CO gas presentation. The immersion in the sensor reaction past 100 ppm of CO gas credited to constrained response destinations existing on the film surface. The temperature-subordinate sensor reaction of Al doped ZnO thin films was contemplated in the temperature scope of 100-300°C to discover the ideal working temperature for CO sensing.

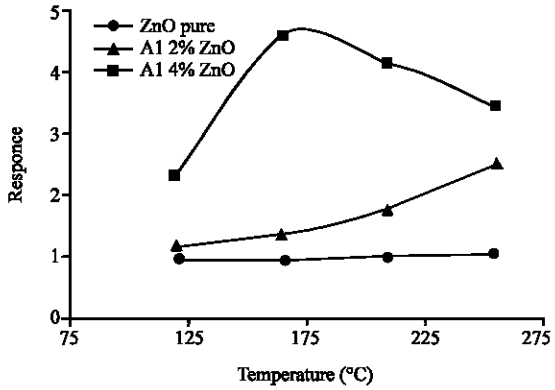

Fig. 6: Sensor response vs. temperature for ZnO:Al thin films

Figure 6 explain the sensor reactions as a function of temperature. The sensor response of 4 wt% Al is phenomenal at 175°C, though ZnO thin films demonstrated sensor response at higher working temperature ~275°C. The sensitivity conduct of thin films have been considered for various concoction inputs.

CONCLUSION

We examined the effect of crystallite size, stacking deformity and higher surface roughness on the sensor response of ZnO doped with Al by using CSP. The CSP method has given pinhole free thin films with a uniform dispersion of grains and well disciple nanocrystalline ZnO based thin films. Deposited films have affirmed the polycrystalline nature with wurtzite hexagonal structure and favored introduction along (002) plane. AFM and SEM showed spherical growth of ZnO:Al grains. The 4 wt% Al doped ZnO sensor shows high response to CO. Best outcomes were achieved in 4 wt% Al doped ZnO sensor at 175°C. The extensive surface area, higher surface roughness and all the more stacking deformities are in charge of upgraded sensor response to CO gas.

REFERENCES

Benharrats, F., K. Zitouni, A. Kadri and B. Gil, 2010. Determination of piezoelectric and spontaneous polarization fields in quantum wells grown along the polar <0001> direction. Superlattices Microstructures, 47: 592-596.

Cao, J. and J. Wu, 2011. Strain effects in low-dimensional transition metal oxides. Mater. Sci. Eng. R. Rep., 71: 35-52.

Chen, D., Y. Zhao, Y. Chen, B. Wang and H. Chen *et al*., 2015. One-step chemical synthesis of ZnO/graphene oxide molecular hybrids for high-temperature thermoelectric applications. ACS. Appl. Mater. Interfaces, 7: 3224-3230.

Diyatmika, W., J.P. Chu, B.T. Kacha, C.C. Yu and C.M. Lee, 2015. Thin film metallic glasses in optoelectronic, magnetic and electronic applications: A recent update. Curr. Opin. Solid State Mater. Sci., 19: 95-106.

Djurisic, A.B., X. Chen, Y.H. Leung and A.M.C. Ng, 2012. ZnO nanostructures: Growth, properties and applications. J. Mater. Chem., 22: 6526-6535.

Fan, F., Y. Feng, S. Bai, J. Feng and A. Chen *et al*., 2013. Synthesis and gas sensing properties to NO2 of ZnO nanoparticles. Actuators B. Chem., 185: 377-382.

Gaspera, E.D., M. Guglielmi, A. Martucci, L. Giancaterini and C. Cantalini, 2012. Enhanced optical and electrical gas sensing response of sol-gel based NiO-Au and ZnO-Au nanostructured thin films. Sens. Actuators B Chem., 164: 54-63.

Hameed, A.S.H., C. Karthikeyan, A.P. Ahamed, N. Thajuddin and N.S. Alharbi *et al*., 2016. In vitro antibacterial activity of ZnO and Nd doped ZnO nanoparticles against ESBL producing Escherichia coli and Klebsiella pneumonia. Sci. Rep., 6: 1-11.

Hasan, N.B. and M.A. Mohammed, 2015. Optical characterization of (PbO)1-x(CdO)x deposited by spray pyrolysis technique. J. Electron. Devices, 22: 1924-1929.

He, Z. and X. Wang, 2015. Renewable energy and fuel production over transition metal oxides: The role of Oxygen defects and acidity. Catal. Today, 240: 220-228.

Huang, J., Z. Yin and Q. Zheng, 2011. Applications of ZnO in organic and hybrid solar cells. Energy Environ. Sci., 4: 3861-3877.

Huang, J.H., T.Y. Huang, H.Y. Wei, K.C. Ho and C.W. Chu, 2012. Wet-milled transition metal oxide nanoparticles as buffer layers for bulk heterojunction solar cells. RSC. Adv., 2: 7487-7491.

Kaur, J., S.C. Roy and M.C. Bhatnagar, 2007. Highly sensitive SnO2 thin film NO2 gas sensor operating at low temperature. Sensors Actuators B, 123: 1090-1095.

Kim, H., A. Pique, J.S. Horwitz, H. Murata, Z.H. Kafafi, C.M. Gilmore and D.B. Chrisey, 2000. Effect of aluminum doping on zinc oxide thin films grown by pulsed laser deposition for organic light-emitting devices. Thin Solid Films, 377-378: 798-802.

Kumar, M., A. Kumar and A.C. Abhyankar, 2014. SnO2 baseds sensors with improved sensitivity and response-recovery time. Ceram. Intl., 40: 8411-8418.

Li, S., Z. Sun, R. Li, M. Dong and L. Zhang *et al*., 2015. ZnO nanocomposites modified by hydrophobic and hydrophilic silanes with dramatically enhanced tunable fluorescence and aqueous ultrastability toward biological imaging applications. Sci. Rep., 5: 1-8.

Li, Z., R. Yang, M. Yu, F. Bai and C. Li *et al*., 2008. Cellular level biocompatibility and biosafety of ZnO nanowires. J. Phys. Chem. C, 112: 20114-20117.

Lin, W.H., T.F.M. Chang, Y.H. Lu, T. Sato and M. Sone *et al*., 2013. CO2-Assisted electrochemical deposition of ZnO mesocrystals for practical photoelectrochemical applications. J. Phys. Chem. C, 117: 25596-25603.

Mandal, D., M.E. Bolander, D. Mukhopadhyay, G. Sarkar and P. Mukherjee, 2006. The use of microorganisms for the formation of metal nanoparticles and their application. Applied Microbiol. Biotechnol., 69: 485-492.

Masuda, Y., T. Itoh, W. Shin, and K. Kato, 2015. SnO2 Nanosheet/Nanoparticle detector for the sensing of 1-nonanal gas produced by lung cancer. Sci. Rep., 5: 1-7.

Nasser, S.A., H.H. Afify, S.A. El-Hakim and M.K. Zayed, 1998. Structural and physical properties of sprayed Copper-Zinc Oxide films1. Thin Solid Films, 315: 327-335.

Poongodi, G., R.M. Kumar and R. Jayavel, 2015. Structural, optical and visible light photocatalytic properties of nanocrystalline Nd doped ZnO thin films prepared by spin coating method. Ceram. Intl., 41: 4169-4175.

Schmidt-Mende, L. and J.L. MacManus-Driscoll, 2007. ZnO-nanostructures, defects and devices. Mater. Today, 10: 40-48.

Tang, X., E.S.G. Choo, L. Li, J. Ding and J. Xue, 2010. Synthesis of ZnO nanoparticles with tunable emission colors and their cell labeling applications. Chem. Mater., 22: 3383-3388.

Tsay, C.Y. and W.T. Hsu, 2013. Sol-gel derived undoped and boron-doped ZnO semiconductor thin films: Preparation and characterization. Ceram. Intl., 39: 7425-7432.

Vasilopoulou, M., L.C. Palilis, D.G. Georgiadou, P. Argitis and S. Kennou *et al.*, 2011. Tungsten oxides as interfacial layers for improved performance in hybrid optoelectronic devices. Thin Solid Films, 519: 5748-5753.

Wang, J., Y.J. Lee and J.W. Hsu, 2014. One-step synthesis of ZnO nanocrystals in N-butanol with bandgap control: Applications in hybrid and organic photovoltaic devices. J. Phys. Chem. C, 118: 18417-18423.

Willander, M., M.Q. Israr, J.R. Sadaf and O. Nur, 2012. Progress on one-dimensional Zinc Oxide nanomaterials based photonic devices. Nanophotonics, 1: 99-115.

Yang, P.F., H.C. Wen, S.R. Jian, Y.S. Lai and S. Wu *et al.*, 2008. Characteristics of ZnO thin films prepared by radio frequency magnetron sputtering. Microelectron. Reliab., 48: 389-394.

Zhang, J., X. Liu, G. Neri and N. Pinna, 2016. Nanostructured materials for room-temperature gas sensors. Adv. Mater., 28: 795-831.